

Fracture Mechanics Analysis of the Single-Fiber Pull-Out Test and the Microbond Test Including The Effects of Friction and Thermal Stresses

John A. Nairn, Chun-Hsin Liu, David.-A. Mendels, Serge Zhandarov

Submitted: June 7, 2001

ABSTRACT

The energy release rate for propagation of a debond in either a single-fiber pull-out test or a microbond test was derived analytically. The key finding was that an accurate analysis can be derived by a global energy analysis that includes effects of residual stresses and interfacial friction but does not need to include the details of the stress state at the interfacial crack tip. The analytical results were verified by comparison to finite element analyses. The energy release rate expressions were used to determine interfacial fracture toughness from single-fiber pull-out tests or microbond tests. The experiments included both macro-sized model microbond specimens (steel wire/epoxy) and micro-sized pull-out and microbond specimens (glass fiber/epoxy or vinyl ester). In all experiments, it was critical to correctly account for the true level of residual stresses in the specimen; in some experiments, the inclusion of friction was also critical. For experiments involving physical aging conditions, it was essential to additionally account for partial relaxation of internal stresses.

INTRODUCTION

Two popular interface characterization tests are the microbond test [1] and the single-fiber pull-out test [2]. In the microbond test, a small droplet of matrix is deposited on a fiber and sheared off by restraining the droplet while the fiber is pulled. In the single-fiber pull-out test, the end of a fiber is embedded in a larger amount of matrix and pulled out while the matrix is held (see Fig. 1). In both experiments, the peak force, P , required to debond the fiber is recorded as a function of droplet length (microbond test) or embedded fiber length (pull-out

John A. Nairn and Chun-Hsin Liu, Mat. Sci. & Engr., Univ. of Utah, Salt Lake City, UT, 84112, USA.

David.-A. Mendels, National Physical Laboratory, Teddington, Middlesex, TW11 0LW, UK.

Serge Zhandarov, Metal-Polymer Research Institute, Kirov Str. 32a, Gomel 246050, Republic of Belarus.

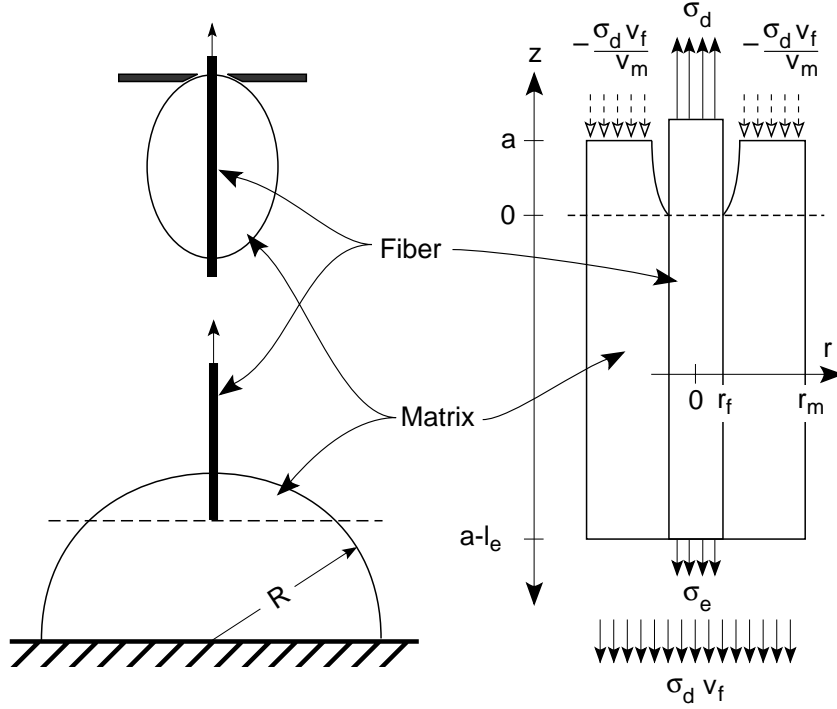


Figure 1. The left side shows the microbond (top) and pull-out (bottom) specimen geometries. The right side shows the equivalent concentric cylinder model where the embedded length of fiber is in a cylinder of matrix. The fiber in both specimens is loaded with stress σ_d . The “dotted” arrows are the remaining microbond specimen boundary conditions; the solid arrows on the bottom of the specimen are the remaining pull-out specimen boundary conditions.

test). A common interpretation of such experiments is to calculate an interfacial shear strength from

$$\tau_{ISS} = \frac{P}{2\pi r_f l_e} \quad (1)$$

where r_f is the fiber radius and l_e is the embedded fiber length. Physically this term is the average interfacial shear stress at the time of failure. It might be useful for qualitative work, but it has several limitations when one desires more rigorous interfacial characterization.

One approach to deriving more fundamental results about interfacial properties is to characterize interfacial failure using fracture mechanics [3–8]. In a fracture mechanics approach, both the microbond and pull-out tests can be viewed as tests that initiate and propagate a crack, in the form of an interfacial debond, along the fiber/matrix interface. To apply fracture mechanics methods, one needs to record the load required for crack growth as a function of current crack length and other relevant specimen geometry variables. The experimental observations need to be reduced to fracture mechanics parameters by calculating the energy release rate for crack growth. This paper summarizes a new analytical result for the energy release rate due to interfacial debond growth in either the microbond or the pull-out test. We have used the new fracture

mechanics methods to interpret microbond and pull-out test results in terms of an interfacial fracture toughness. The analysis methods account for both the effects of residual stresses and interfacial friction. It was found that both effects are important and must be included before valid fracture mechanics results can be derived from interfacial tests.

THEORY

Figure 1 shows a reduction of both a real microbond specimen and a real pull-out specimen to an idealized geometry using concentric cylinders [4, 5, 6]. For the pull-out test, there are three simplifications. First, the restraint on the bottom of the matrix is replaced by a uniform traction that balances the traction applied to the top of the fiber. Second, the matrix region surrounding the embedded fiber is replaced by an equivalent cylinder of matrix whose radius is chosen to preserve the total amount of matrix material within the zone of the embedded fiber. Third, because the free fiber length, before the fiber enters the matrix, and the free matrix zone, below the bottom of the embedded fiber, are under constant-traction, they release no energy as the debond propagates [6]. The energy release rate analysis can thus focus on the concentric cylinder model on the right of Fig. 1. The length of the concentric cylinders is equal to the embedded fiber length, l_e . By equating the volume of the specimen above the bottom of the embedded fiber (the zone above the dotted line in the pull-out specimen in Fig. 1) to the volume of the equivalent cylinder, the effective matrix outer radius can be calculated from [6]:

$$r_m = \sqrt{l_e \left(R - \frac{l_e}{3} \right)} \quad (2)$$

where R is the radius of the typically hemispherical pull-out specimen droplet. The effective fiber volume fraction is $v_f = r_f^2/r_m^2$. The boundary conditions for the pull-out test are shown by the solid arrows. The fiber is pulled with a stress of σ_d . By force balance, the total stress on the bottom of the specimen is $\sigma_0 = v_f\sigma_d$. The stress σ_e shown on the bottom of the fiber is the actual internal stress on the end of the embedded fiber.

For the microbond specimen, there are two simplifications. First, the elliptical matrix droplet is replaced by a matrix cylinder with length equal to the embedded fiber length and matrix radius chosen to preserve the total fiber volume fraction within the matrix. An important experimental observation in micro-sized microbond specimens is that the effective fiber volume fraction changes as the droplet length increases; this effect needs to be included in any fracture mechanics analysis of microbond results [7]. Second, the constant displacement boundary conditions in real specimens, in which the matrix is restrained while the fiber is pulled, are replaced by constant traction boundary conditions that balance the stress applied to the fiber. The microbond specimen boundary conditions thus include the fiber stress of σ_d at the top of the specimen; that stress

is balanced by a matrix stress (shown with dotted lines in Fig. 1) of $-\sigma_d v_f / v_m$. The bottom of a microbond specimen is stress free ($\sigma_e = \sigma_0 = 0$).

Using the general composite fracture mechanics methods from Ref. [8] and applying them to the geometry in Fig. 1 with an interfacial debond of length a , the energy release rate for debond growth in both the pull-out and microbond specimens can be written as [6]:

$$G(a) = \frac{r_f}{2} \left\{ C_{33s} \bar{\sigma}^2 + 2D_{3s} \bar{\sigma} \Delta T + \left(\frac{D_3^2}{C_{33}} + \frac{v_m (\alpha_T - \alpha_m)^2}{v_f A_0} \right) \Delta T^2 - \left[\frac{\sigma_0}{2} \left(\frac{1}{E_A} - \frac{1}{E_m} \right) + D_{3s} \Delta T \right] \times \left[\frac{2\tau_f}{r_f} C_T(a) - \left(\bar{\sigma} + \frac{(1+m)D_3 \Delta T}{C_{33}} \right) C'_T(a) \right] \right\} \quad (3)$$

where $m = 0$ is used for a pull-out test and $m = 1$ is used for a microbond stress. The term $\bar{\sigma}$ is a reduced debonding stress defined by

$$\bar{\sigma} = \sigma_d - \frac{2\tau_f a}{r_f} - \frac{\sigma_0 E_A}{v_f E_A + v_m E_m} \quad (4)$$

Other terms in Eq. (3) are fiber radius, volume fraction, transverse thermal expansion coefficient, and axial modulus (r_f , v_f , α_T , and E_A), matrix volume fraction, thermal expansion coefficient, and modulus (v_m , α_m , and E_m), a temperature difference which defines the level of residual stresses (ΔT), a friction stress on the debond (τ_f), a stress-transfer function ($C_T(a)$), and several constants which depend only on the fiber and matrix properties and the geometry of the concentric cylinders (C_{33s} , D_{3s} , A_0 , D_3 , and C_{33} which are defined in Ref. [6]). As explained elsewhere [6], Eq. (3) is essentially an exact result for debonding energy release rate in the concentric cylinders model including both the effects of residual thermal stresses and friction. Residual stresses are included by selecting ΔT to match the true level of residual stresses in the specimen. Because rigorous modeling of Coulomb friction is difficult, friction is included in an approximate manner. It is included by introducing a constant shear stress on the debond surface of τ_f . This frictional stress contributes to energy release rate by external work on the debond surfaces as the fiber and matrix slide by each other. In some experiments it is possible to measure τ_f [5] and thus we claim this approach can accurately include friction effects.

Although Eq. (3) can be demonstrated to be accurate, it is written in terms of the solution to an elasticity problem. The cumulative stress transfer function $C_T(a)$ is define by:

$$C_T(a) = \int_0^{l_e - a} F(z) dz \quad (5)$$

where the function $F(z)$ is the solution to an underlying stress-transfer problem; it is the average axial fiber stress in concentric cylinders of length $l_e - a$ subjected to unit normal stress on the fiber and a balancing $-v_f/v_m$ stress on the matrix, both at $z = 0$ in addition to zero stress on the other end at $z = l_e - a$. The

function $F(z)$ and therefore $C_T(a)$ can be found by any analytical, numerical, or even experimental means and then substituted into Eq. (3) to find energy release rate. One simple analytical approach is to use shear lag analysis for which it is easy to derive [5]:

$$C_T(a) = \frac{1}{\beta} [\coth \beta(l_e - a) - \operatorname{csch} \beta(l_e - a)] \quad (6)$$

$$C'_T(a) = -\frac{1}{2} \operatorname{sech}^2 \left(\frac{\beta(l_e - a)}{2} \right) \quad (7)$$

where β is the shear-lag parameter most accurately defined by [9, 10, 11]

$$\beta^2 = \frac{2}{r_f^2 E_A E_m} \left[\frac{E_A v_f + E_m v_m}{\frac{v_m}{4G_A} + \frac{1}{2G_m} \left(\frac{1}{v_m} \ln \frac{1}{v_f} - 1 - \frac{v_f}{2} \right)} \right] \quad (8)$$

and G_A and G_m are the axial shear modulus of the fiber and shear modulus of the matrix.

Two interesting limits of Eq. (3) are when the embedded fiber length is long and when the interface is frictionless. For long embedded fibers, the function $F(z)$ will decay from $F(z) = 1$ at $z = 0$ to $F(z) = 0$ long before the end of the bonded interface zone at $z = l_e - a$. Clearly, this limit implies $C_T(a)$ is a constant which further implies that $C'_T(a) = 0$. Writing the constant as $C_T(a) = 1/\beta$ (which is also the long-fiber limit of the shear-lag solution), the long-fiber limiting result is

$$G_\infty(a) = \frac{r_f}{2} \left\{ C_{33s} \bar{\sigma}^2 + 2D_{3s} \bar{\sigma} \Delta T + \left(\frac{D_3^2}{C_{33}} + \frac{v_m (\alpha_T - \alpha_m)^2}{v_f A_0} \right) \Delta T^2 - \frac{2\tau_f}{r_f \beta} \left[\frac{\sigma_0}{2} \left(\frac{1}{E_A} - \frac{1}{E_m} \right) + D_{3s} \Delta T \right] \right\} \quad (9)$$

The frictionless limit for any fiber length or for long fiber lengths can easily be found by setting $\tau_f = 0$ in Eq. (3) or Eq. (9), respectively. Note that for the combination of frictionless interfaces and long fibers that all terms involving $C_T(a)$ and $C'_T(a)$ drop out. In other words, for this special case, energy release rate can be determined without the need for any stress analysis to find $C_T(a)$.

EXPERIMENTAL RESULTS

Comparison to Finite Element Analysis

The accuracy of the analytical equation for energy release rate can be checked by comparison to finite element results, as shown in Fig. 2. This comparison was for glass fibers embedded in a polymer matrix. The fiber radius was $r_f = 10.5 \mu\text{m}$, had an embedded length of $420 \mu\text{m}$, and specimen volume fraction of $v_f = 1\%$. The specimen was loaded with $\sigma_d = 400 \text{ MPa}$, thermal load

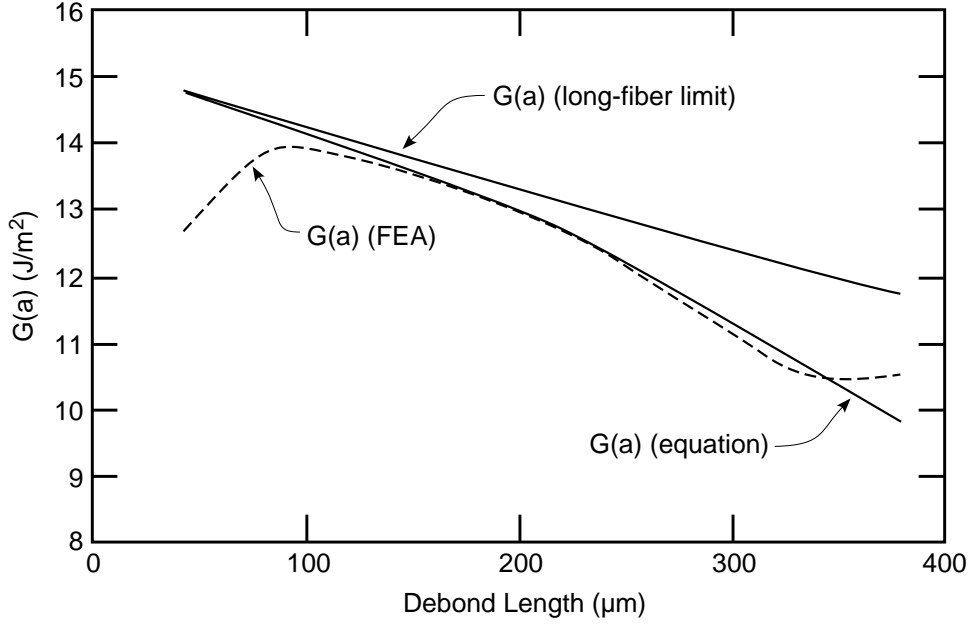


Figure 2. A sample calculation of $G(a)$ for a single-fiber pull out test. The “equation” results are from Eq. (3); the “long-fiber limit” results are from Eq. (9); the dashed line is the result of finite element calculations.

$\Delta T = -100^\circ\text{C}$, and interfacial friction of $\tau_f = 1 \text{ MPa}$. The finite element analysis used axisymmetric, 8-noded, isoparametric elements. The energy release rate as a function of debond length was found by a modified crack closure technique [12]. The analytical results are for both the full analysis in Eq. (3) and for the long-fiber limit in Eq. (9). The full analysis and the finite element analysis agree extremely well provided the debond length is neither too long nor too short. Some approximations used here relied on the debond tip not being too close to either end. The results in Fig. 2 show that when that condition holds the analytical result is very accurate. When the debond tip is near either end, the finite element analysis and the analytical result disagree. It is not certain, however, that the finite element results should be viewed as correct in these extremes. The finite element analysis has its own set of problems when the debond tip gets too close to boundaries. The analytical solution, which is smoother, may even provide a better representation of the energy release rate as a function of debond length than the finite element analysis. This issue could be resolved by more refined finite element analysis. The long-fiber limit agrees well with the full analysis and with finite element analysis only for the shorter debond lengths. As the debond length increases, the term $l_e - a$ gets smaller and the long-fiber limit becomes increasingly less accurate. It can be shown that the long-fiber limit requires $l_e - a$ to be about an order of magnitude larger than $1/\beta$ [6]. In this example $1/\beta$ was $28.3 \mu\text{m}$.

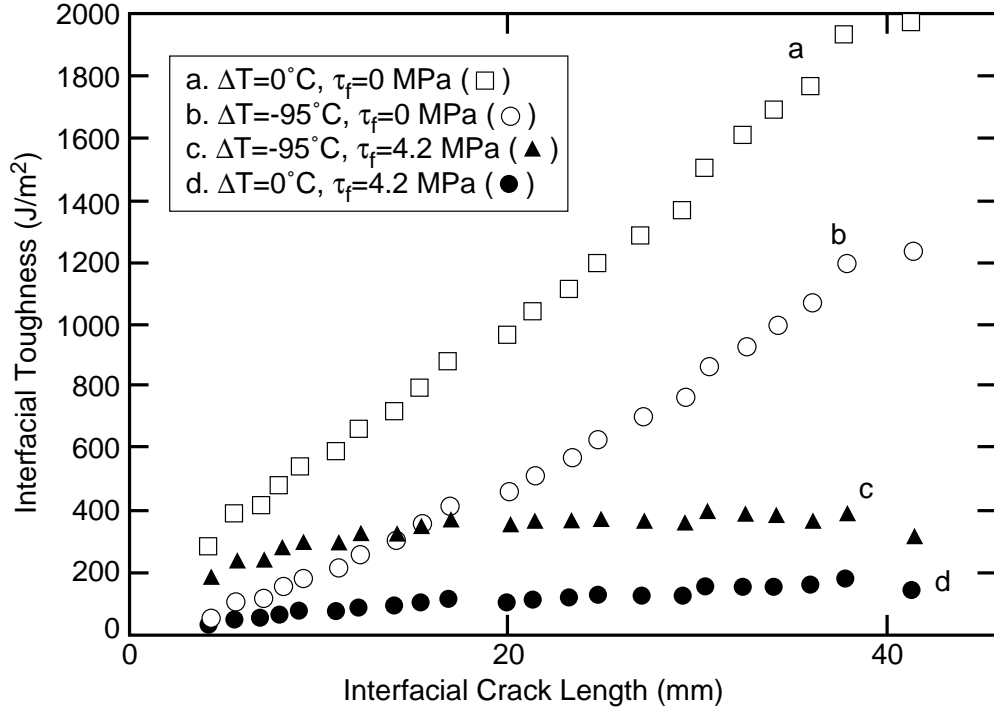


Figure 3. Crack-resistance curves for a steel/epoxy model specimen analyzed four different ways. Curve *a* ignores residual stresses and friction; curve *b* includes residual stresses but ignores friction; curve *c* includes both residual stresses and friction; curve *d* ignores residual stresses, but includes friction.

Model Experiments

For verification of the use of Eq. (3) for analysis of debonding experiments, we did model experiments for steel wire embedded in epoxy cylinders [5]. There were three advantages to these model specimens. First, the specimen geometry could be fabricated to closely match the concentric cylinder geometry used in the analysis. Second, it was possible to observe stable debond propagation and thus from a single specimen we were able to record many results for failure load as a function of crack length. Third, after complete debonding the epoxy cylinder slid along the fiber restrained only by friction. We were able to record the friction stress and use that result for the friction term in the energy release rate analysis. In brief, epoxy cylinders were molded around steel wires. The model microbond experiment was to thread the wire through a hole in a steel plate and pull on the wire while the plate restrained the epoxy cylinder. By using back lighting, we could monitor crack growth and record fiber stress, σ_d , as a function of debond length, a . All experimental results were then substituted into Eq. (3) to calculate $G(a)$ or the interfacial fracture toughness. If a fracture mechanics analysis of these experiments is valid, the toughness should be a material property that is independent of the debond length.

Figure 3 give the results of analyzing model experiments by various combi-

nations of including or not including thermal stresses and/or friction. Curve *a* is an analysis that ignores both residual stresses and interfacial friction. This curve is clearly a poor fracture mechanics result; it is never constant. Curve *b* includes residual thermal stresses by setting $\Delta T = -95^\circ\text{C}$ (which is close to the temperature difference between the post-cure temperature and the testing temperature), but still ignores friction. Again, curve *b*, is a poor fracture mechanics result. Curves *c* and *d* (filled symbols in Fig. 3) both include friction effects by setting $\tau_f = 4.2$ MPa which was the measured interfacial shear stress after complete debonding. Curve *c* is an analysis that included both residual stresses and friction. This curve is a good fracture mechanics result. There is evidence for an initial rise in toughness at short debond lengths, but the *R*-curve soon levels out at an approximately constant value of about 360 J/m². This value for toughness is a reasonable result for a steel/epoxy interface. Curve *d* includes interfacial friction, but ignores residual stresses. Although curve *d* looks relatively flat on the scale of Fig. 3, it actually never levels off and is a poor fracture mechanics result. The difference between curves *c* and *d* illustrates the magnitude of the contribution of residual stress to debonding. The magnitude is large; in fact, most of the energy released comes from residual stresses.

The model experiments show that Eq. (3) can be used to analyze microbond experiments using fracture mechanics. The results also show the importance of including both friction and residual stresses in that analysis. Without friction, the energy release rate is not constant. In other words, the work of frictional sliding needs to be subtracted before one can get a true result for interfacial toughness. Once friction is correctly included, most of the remaining energy released comes from the release of residual stresses. In other words, residual stresses play an important role in interfacial failure of microbond specimens. For microbond specimens to be useful for determining interfacial failure properties, it is essential that the analysis method account for residual stresses. This point is illustrated further in the next example.

Physical Aging

We also did experiments on micro-sized, glass-fiber/epoxy microbond specimens and interpreted the results using fracture mechanics [13]. There are two new difficulties in micro specimens *vs.* model specimens. First, the droplets assume a natural elliptical shape and can not be molded into cylinders. We analyzed experiments with elliptical droplets by setting the radius of the equivalent matrix cylinder to give the same volume of matrix as in the real specimen. The volume of the matrix in the real specimens can be found from the length and diameter of the elliptical droplet. From such measurements, it has been observed that fiber volume fraction within the droplet varies with embedded fiber length [7]. Many older microbond experiments recorded results only as a function of fiber length and did not report droplet diameter. Because it is not possible to deduce the changes in fiber volume fraction in such results, these older results are not amenable to reinterpretation by fracture mechanics.

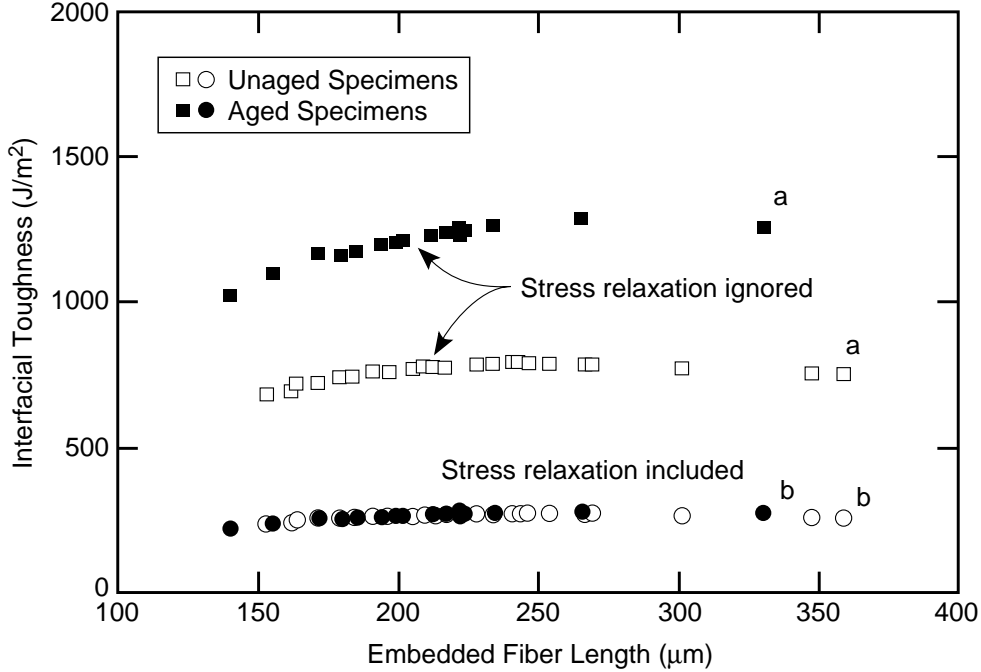


Figure 4. Fracture toughness calculated from microbond specimens as a function of droplet length. Curves *a* include residual stresses but do not account for relaxation of those stresses during processing or aging. Curves *b* account for relaxation of residual stresses.

The second difficulty with real microbond specimens is observation of crack length — it is difficult or impossible to observe crack growth. From our energy release rate analysis in the presence of friction, however, the prediction is that the interfacial debond should grow stably as the load increases to the peak load. As a consequence, the peak load, which is typically measured, corresponds to a droplet of length l_e in which $a \approx l_e$ or in which the crack is near the point of complete debonding [5]. This prediction agrees with the results from model experiments. In a previous paper [5], we suggested that interfacial toughness in microbond experiments that lack crack observations can be calculated by using the peak load, assuming $a = l_e$, and calculating $G(a)$ from the long-fiber limit in Eq. (9) or from $G_\infty(l_e)$. The long-fiber limit is used instead of the actual limit because Eq. (3) becomes less accurate for $a \approx 0$ or $a \approx l_e$. In contrast, Eq. (9) is well behaved and was shown in model experiments to give good results for toughness when $a \approx l_e$.

In brief, we did a series of experiment for glass fibers embedded in a low T_g epoxy matrix. For each specimen, we recorded the embedded fiber length, matrix droplet diameter, the peak load at debonding, and the frictional load after debonding. Some specimens were tested immediately after fabrication (the “unaged” specimens). Other specimens were aged for 3 days at 37°C (which was $T_g - 5.1^\circ\text{C}$) before testing [13]. The experimental results were substituted into Eq. (9) using $a = l_e$ to find toughness and are plotted as a function of droplet length in Fig. 4. Good fracture mechanics results should show a toughness that

is independent of droplet length and differences between unaged and aged results should show the affect of physical aging on the interfacial fracture toughness.

The one parameter not directly measurable by experimental observations was ΔT which determines the level of residual stresses. The model experiments demonstrated the importance of including residual stresses in analysis of microbond tests. Their correct inclusion was similarly vital to a valid fracture mechanics interpretation of micro-sized specimens. The curves labeled “a” in Fig. 4 were calculated by a simple thermoelastic analysis for residual stresses that basically takes ΔT close to test temperature minus the T_g of the matrix [13]. Because of the low T_g of this epoxy, however, there is a possibility of stress relaxing while cooling. Furthermore, the aging conditions will allow further stress relaxation. From viscoelastic modeling of the thermal history of all samples, we calculated a more realistic ΔT that accounts for all stress relaxation and used that result to calculate interfacial toughness [13]. The results are in the curves labeled “b”. These results provide an interfacial fracture toughness of $264 \pm 15 \text{ J/m}^2$ that is both independent of droplet length (as expected in fracture mechanics) and independent of aging time. In other words, aging relaxes internal stresses, but it has no effect on interfacial fracture toughness. Any attempt to study aging effects with analysis methods that do not correctly account for residual stresses will likely lead to erroneous conclusions about the effect of aging on interfacial properties.

Pull Out

We also used fracture mechanics to analyze pull-out tests for glass fibers of various diameters embedded in a vinyl ester matrix [14]. In the pull-out apparatus, we were able to observe an initial kink in the load-displacement curve. This kink was taken to be the point of initiation of debonding. For each specimen, we thus recorded embedded fiber length, droplet radius (R in Fig. 1), and the fiber stress at debond initiation. These results were substituted into Eq. (3) using $a = 0$ and calculating ΔT from the curing conditions. Friction was ignored in these experiments because we only considered initiation. The effect of friction only becomes significant as the debond length gets long. The calculated interfacial toughness for three fibers of different diameters are plotted in Fig. 5 as a function of embedded fiber length. After an initial rise, the results for all three fibers became roughly constant at $15 \pm 3 \text{ J/m}^2$. In other words, as expected for good fracture mechanics results, the interfacial toughness was independent of both fiber length and fiber diameter. Additional fracture mechanics analyses for different matrices and different fiber/matrix interfacial conditions are given in Ref. [14]. The results always gave toughnesses that were independent of embedded fiber length, but were not always independent of fiber diameter. Reference [14] proposed an alternate analysis method based on peak shear stress at the point of initiation. Provided the shear stresses analysis included effects of non-uniform shear stress and residual stresses, it gave good results for all experiments.

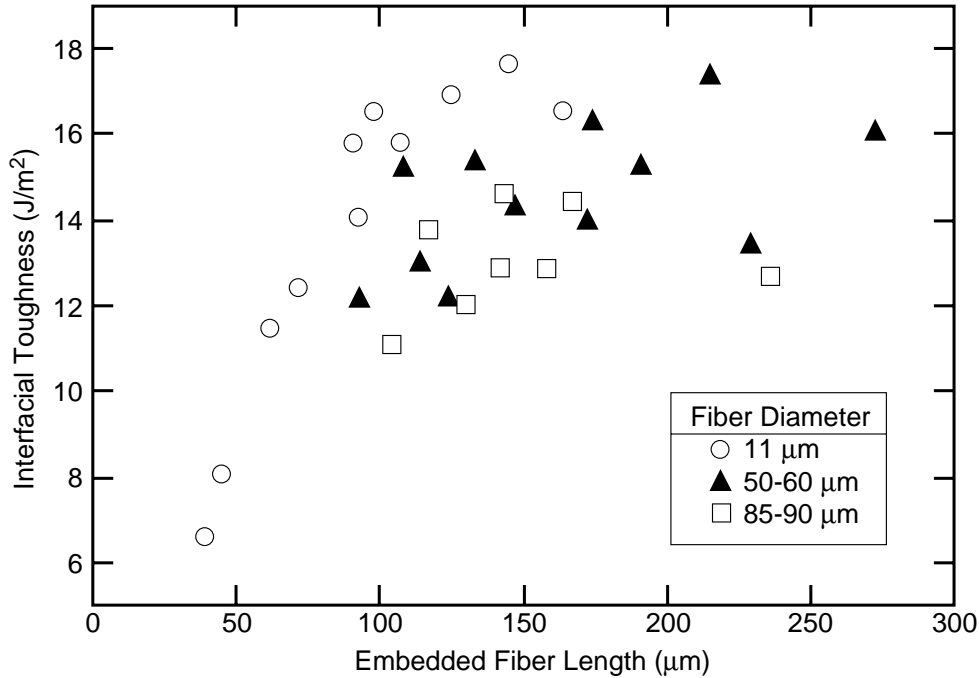


Figure 5. Fracture toughness calculated from initiation of debonding in pull-out tests for glass fibers of three different diameters in a vinyl-ester matrix as a function of embedded fiber length.

CONCLUSIONS

Equation (3) provides an accurate, analytical result that can be used to calculate the energy release rate for interfacial crack growth in both the microbond and the single-fiber pull-out test geometries. The experiments presented in this paper show that this equation can be used to derive fracture toughness information from these common interfacial test methods. The calculation of interfacial toughness, however, requires sufficient experimental input for determination of all terms in Eq. (3). The key results needed are specimen geometry, current interfacial crack length, the load required to extend the crack, the actual level of residual stresses, and the magnitude of any friction on the debond surfaces. Residual stresses are particularly important for analysis of microbond specimens because they account for much of the energy released. We would not have been able to interpret the effects of physical aging if our analysis did not correctly account for all residual stresses and for relaxation of residual stresses during processing or aging. Similarly, friction is important, especially as the debond gets long. Without proper inclusion of friction effects, it would not be possible to find a meaningful interfacial fracture toughness that is independent of crack length. In some micro-sized specimens it can be difficult to observe crack growth. This situation can sometimes be handled by using other means to deduce crack length. For example, we deduced that the crack length at the peak load in microbond tests is nearly equal to the droplet length. For pull-out tests,

we were able to observe debond initiation as a kink in the force-displacement curve and thus the “kink” load corresponds to zero initial crack length.

Acknowledgements

This work was supported, in part, by a grant from the Mechanics of Materials program at the National Science Foundation (CMS-9713356).

REFERENCES

1. Miller, B., P. Muri, and L. Rebenfeld. 1987. “A Microbond Method for Determination of the Shear Strength of a Fiber/Resin Interface,” *Comp. Sci. & Tech.*, 28:17–32.
2. Penn, L. S., and E. R. Bowler. 1981. “A New Approach to Surface Energy Characterization for Adhesive Performance Prediction,” *Surf. Interf. Anal.*, 3:161–164.
3. Nairn, J. A., and Y. C. Liu. 1996. “On the Use of Energy Methods For Interpretation of Results from Single-Fiber Fragmentation Experiments,” *Comp. Interfaces*, 4:241–267.
4. Scheer, R. J., and J. A. Nairn. 1992. “Variational Mechanics Analysis of the Stresses and Failure in Microdrop Debond Specimens,” *Composites Engineering*, 2:641–654.
5. Liu, C. H., and J. A. Nairn. 1999. “Analytical Fracture Mechanics of the Microbond Test Including the Effects of Friction and Thermal Stresses,” *J. of Adhes. and Adhesives.*, 19:59–70.
6. Nairn, J. A. 2000. “Analytical Fracture Mechanics Analysis of the Pull-Out Test Including the Effects of Friction and Thermal Stresses,” *Adv. Comp. Letts.*, 9:373–383.
7. Scheer, R. J., and J. A. Nairn. 1995. “A Comparison of Several Fracture Mechanics Methods for Measuring Interfacial Toughness with Microbond Tests,” *J. Adhesion*, 53:45–68.
8. Nairn, J. A. 2000. “Exact and Variational Theorems for Fracture Mechanics of Composites with Residual Stresses, Traction-Loaded Cracks, and Imperfect Interfaces,” *Int. J. Fract.*, 105:243–271.
9. Nairn, J. A. 1997. “On the Use of Shear-Lag Methods for Analysis of Stress Transfer in Unidirectional Composites,” *Mech. of Materials*, 26:63–80.
10. McCartney, L. N. 1992. “Analytical Models of Stress Transfer in Unidirectional Composites and Cross-Ply Laminates, and Their Application to the Prediction of Matrix/Transverse Cracking,” in *Local Mechanics Concepts for Composite Material Systems*, J. N. Reddy and K. L. Reifsnider, eds., Proc. IUTAM Symposium, pp. 251–282.
11. Nayfeh, A. H. 1977. “Thermomechanically Induced Interfacial Stresses in Fibrous Composites,” *Fibre Sci. & Tech.*, 10:195–209.
12. Krishnamurthy, T., T. S. Ramamurthy, K. Vijayakumar, and B. Dattaguru. 1985. “Modified Crack Closure Integral Method for Higher Order Finite Elements,” presented at the Proc. Int. Conf. Finite Elements in Computational Mechanics, Bombay, India, December 2–6, 1985.
13. Mendels, D.-A., Y. Leterrier, J.-A. E. Månson, and J. A. Nairn. 2001. “The Influence of Internal Stresses on the Microbond Test II: Physical Aging and Adhesion,” submitted.
14. Zhandarov, S., E. Pisanova, E. Mader, and J. A. Nairn. 2000. “Investigation of Load Transfer Between the Fiber and the matrix in Pull-Out Tests with Fibers Having Different Diameters,” *J. Adhesion Sci. & Tech.*, 15:205–222.